ACS APPLIED MATERIALS & INTERFACES

Research Article

www.acsami.org

Microstructural, Electrical, and Mechanical Properties of Graphene Films on Flexible Substrate Determined by Cyclic Bending Test

Ba-Son Nguyen,[†] Jen-Fin Lin,*[,†,‡] and Dung-Ching Perng[‡,§]

[†]Department of Mechanical Engineering, [‡]Center for Micro/Nano Science and Technology, and [§]Institute of Microelectronics and Electrical Engineering Department, National Cheng Kung University, 1 University Road, Tainan 701, Taiwan

ABSTRACT: Three kinds of graphene/polyimide specimen were prepared via transfer with 3, 6, and 9 graphene layers, respectively. A self-designed bending tester was applied to carry out cyclic bending tests with various bending cycles and bending frequencies. The variations of electrical resistance of the specimens during the bending process and the rate of increase of electrical resistance with the number of bending cycles and bending frequency for various total graphene thicknesses were determined. The voids that form at the interfaces between any two adjacent layers increase in size, leading to a disconnection between graphene layers after a number of bending cycles. A reduction in the graphene thickness and increases in the number of bending cycles and bending frequency increase the rate of increase of electrical resistance. For specimens with a given graphene thickness, the I_D/I_G value of the Raman shift increases exponentially with increasing number of bending cycles and bending frequency. An increase in I_D/I_G is accompanied by increases in both the rate of increase of electrical resistance and the aspect ratio L_1/L_2 (where L_1 and L_2 are the half lengths of the long and short axes, respectively, of the selected-area electron diffraction pattern of graphene). The tilt angle formed in the top graphene layer of the specimen after bending tests increases with increasing graphene thickness for a given bending frequency. The rate of increase of the tilt angle is affected by the bending frequency.

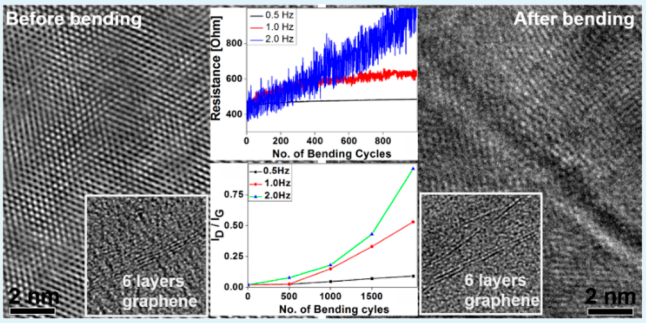

KEYWORDS: *graphene transfer, cyclic bending, bending frequency, void, electrical resistance*

INTRODUCTION

Chemical vapor deposition (CVD) has been applied to deposit large-scale single-layer graphene on metal substrates.[1−5] Nucleation and growth conditions of graphene during the CVD process is important to achieve large, high-quality single crystals. Control of surface oxygen on copper enabled repeatable growth of centimeter-scale single-crystal graphene domains.[6] Graphene films of the order of centimeters on copper substrates with 95% single-layer can be grown by CVD using methane.[7] Bilayer graphene film with an area of at least 5 × 5 cm and bilayer coverage of over 99% has been reported.[8] Roll-to-roll production of 30-in. graphene films has been demonstrated using flexible Cu foils and roll-to-roll transfer technique.[9] Technique of grain boundary stitching[10] or connecting[11] of polycrystalline graphene is also available for better electrical performance. The uniformity, layer number, and stacking order of graphene films can be determined based on a combination of the full width at half-maximum of the 2D band and the peak intensity ratio of 2D band to G band from the Raman spectroscopy.[12−15] Graphene is a promising material for semiconductor devices, with the potential to allow lower-power, faster, and smaller electronics.

Recently, its mechanical properties have been investigated extensively. Scarpa et al.[16] used truss-type analytical models and an approach based on cellular material mechanics theory to describe the in-plane linear elastic properties of a single-layer graphene sheet. These models provided insight into the equivalent mechanical deformation mechanisms when the sheet undergoes small strain uniaxial and pure shear loading. In the study of Ni et al.,[17] tunable uniaxial tensile strain was applied on single- and three-layer graphene by stretching PET in one direction. Raman spectroscopy was used to study the strain effect on graphene. Significant red shifts of the Raman 2D band and G band for single-layer graphene were observed under uniaxial tensile strain. Mohiuddin et al.[18] developed the constitutive relations of graphene and probed the physics of its optical phonons by investigating its Raman spectrum as a function of uniaxial strain. The doubly degenerate E_{2g} optical mode was found to split into two components, namely G^+ and G^-. Both peaks red-shifted with increasing strain and their splitting increased. A Raman mapping investigation of the strain effects on graphene deposited on a transparent flexible substrate was carried out by Yu et al.[19] Raman mapping revealed a significant red-shift of the 2D mode with the introduction of tensile strain, a distribution of local strain, and immediate recovery after strain relaxation. The uniaxial strain

Received: May 27, 2014
Accepted: October 17, 2014
Published: October 17, 2014

broke the sublattice symmetry of graphene, and thus changed its electronic band structures.

The mechanical properties of single-atomic-layer graphyne sheets were characterized by full atomistic first-principles-based ReaxFF molecular dynamics by Cranford and Buehler.[20] Atomistic modeling was carried out to determine the mechanical properties of the graphene sheets for both in-plane and bending deformation, including material failure and intersheet adhesion. The mechanical behavior of graphene flakes under both tension and compression was examined using a cantilever-beam arrangement.[21] The variation of the two components of the 2D peak, namely $2D_1$ and $2D_2$, in bulk graphene was also monitored. The mechanical properties were found to be governed by the strength and stiffness of the interaction bonds.

The movement of dislocations in a crystal is the key mechanism for plastic deformation in all materials. In the study of Warner et al.,[21] the strain fields were determined to show how dislocations deform graphene by elongation and compression of C−C bonds, shear, and lattice rotations. The study of Frank et al.[22] focused on the appearance of defects in graphene grown on Cu (100), (110), and (111) single crystals. By analyzing the Raman D band, they found that the defects originate mainly at the boundaries between Cu (100) and Cu (110); the other main source of defects might be graphene edges. Cyclic strain localization into persistent slip (PS) bands produces on the surface of cyclically deformed materials PS markings in the form of extrusions and intrusions.[23] The localized cyclic plastic strain in PS bands leads to the production and annihilation of dislocations as well as point defects.

Because large-area deposition of graphene sheets is feasible, graphene is also highly elastic and has excellent electrical conductivity,[24] and thus has great potential as an electrode material, especially in the application of flexible optoelectronics. However, its reliability as a flexible electrode material has not been intensively investigated. In this study, three kinds of graphene/polyimide (PI) specimen were prepared via transfer[4] with three graphene thicknesses. A bending tester with reciprocating motion was applied to carry out bending tests with various bending cycles and bending frequencies. Variations of electrical resistance and the rate of increase of $\Delta R/R_o$ ($\Delta R/R_o$, where ΔR is the change in electrical resistance and R_o is the initial electrical resistance) in these specimens during the bending process with number of bending cycles and bending frequency are determined. The effects of the total graphene thickness, number of bending cycles, and bending frequency on $\Delta R/R_o$ are thus evaluated. The voids formed at the interfaces of any two adjacent layers of these specimens before the bending test and their evolutions after bending in terms of size and graphene disconnection are investigated. The effects of graphene thickness, number of bending cycles, and bending frequency on these defects are also evaluated. Raman analysis is used to determine the peak intensities (I) of the D band, G band, and 2D band. The I_D/I_G values are expressed for the 2-transfer specimens as a function of the number of bending cycles and bending frequency. The TEM selected-area electron diffraction (SAED) are used to determine the L_1 and L_2 lengths (L_1 and L_2 are the half lengths of the long and short axes, respectively, of the selected-area electron diffraction pattern of graphene) for these specimens. The relations between I_D/I_G and $\Delta R/R_o$ and L_1/L_2, respectively, are established. The tilt angle of the top layer graphene is measured for specimens with various graphene thicknesses at various bending frequencies.

EXPERIMENTAL DETAILS

An ultrathin graphene film (~1 nm) was grown on a Cu sheet via CVD[23] (Bluestone Tech. Taiwan) and then carefully transferred to a polyimide (PI) substrate. Prior to the film transfer, the substrate was cleaned by soaking in acetone followed by rinsing in deionized water to remove contaminants and then dried under N_2. A layer of poly(methyl methacrylate) (PMMA) was spin-coated to cover the graphene surface as a temporary rigid support during the etching of Cu. The Cu foil was etched away using $FeCl_3$ solution. After the removal of Cu, the PMMA/graphene film was transferred to the PI substrate and the PMMA layer was dissolved carefully in acetone. The graphene thickness was controlled by the number of transfer processes. Specimens (size: 1 × 6 cm) with 1, 2, and 3 graphene trasfers were prepared. The graphene thicknesses of the one-, two-, and three-transfer specimens were 1.1 ± 0.05, 2.3 ± 0.1, and 3.2 ± 0.1 nm, respectively. The specimens were then subjected to a cyclic bending test on a self-designed bending tester (as shown in Figure 1)

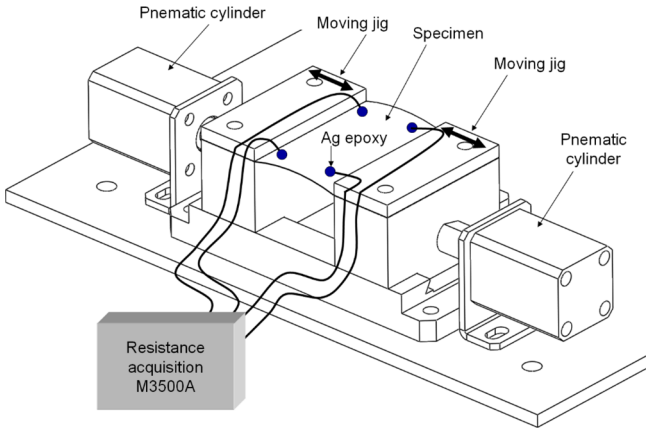

Figure 1. Schematic of Self-Designed Bending Tester.

at three frequencies (0.5, 1.0, and 2.0 Hz) for five numbers of bending cycles (N = 0, 500, 1000, 1500, and 2000). A testing unit in reciprocating motion[25] was adopted to study the fatigue-induced fracture behavior and electrical resistance increase of the graphene film during the bending tests. This self-designed testing unit is suitable for commercial specimens and has no bending cycle number limit. The two jigs connected to the specimen were moved back and forth by controlling the acceleration of motion. An accelerometer was attached near the joint of the moving jig and pneumatic cylinder to measure the acceleration of the jig in one cycle. The jig's maximum acceleration was governed by the air flow fed into the pneumatic cylinders. The acceleration data were acquired and displayed on the computer monitor. The graphene films, before and after cyclic bending, were characterized by a confocal Raman spectroscope (Renishaw InVia, England) using 633 nm laser excitation. Copper wires that connected (using silver expoxy) to both ends of the graphene film were used to measure the electrical resistances of specimens during cyclic bending. The thickness of the graphene films, with an M-bond coating film to protect the graphene layers from damage by the electron or ion beam, was measure with a dual-beam focused ion beam (FIB) (Nova-200 NanoLab). High-resolution transmission electron microscopy (HRTEM, JEOL, JEM-2100F) was used to observe the cross section and thickness of the graphene films, and to characterize their lattice structure before and after cyclic bending.

RESULTS AND DISCUSSION

In the present study, graphene/PI specimens were prepared with three thicknesses via transfer from graphene. The actual

number of graphene layers and film thickness were identified from the TEM morphology of the specimen's cross section prepared by a FIB. The morphologies of the three kinds of sample before cyclic bending are shown in Figures 2a–c,

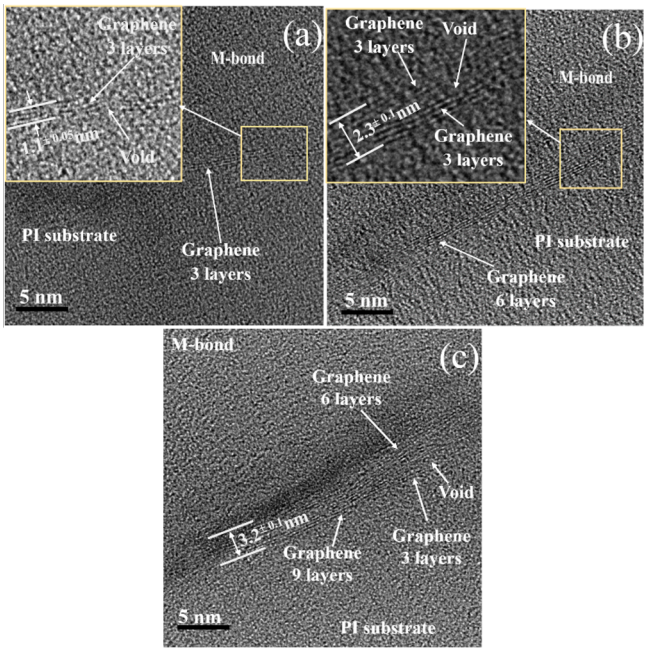

Figure 2. TEM morphologies of lateral surfaces of specimens prepared with (a) 1, (b) 2, and (c) 3 transfers before bending test.

respectively. In Figure 2a, for the sample prepared with one transfer, 3 layers of graphene can be observed lying between the PI substrate and the M-bond coating. A shuttle-shaped void formed at the interface between the PI substrate and the bottom layer of graphene, where a bulge formed, prompting the graphene layers to turn around. For the specimen prepared with two transfers, shown in Figure 2b, 6 layers of graphene can be observed. The upper-left corner shows the magnification of the morphology where a shuttle-shaped void formed at the interface between the upper three layers (from the second transfer) and the lower three layers of graphene (from the first transfer). These voids may come from the transfer process or the PMMA residue on the graphene surface after each time of transfer. Figure 2c shows the cross-sectional morphology of the specimen prepared with three transfers. A total of 9 layers of graphene were deposited. Similar to the previous two specimens, voids formed at the interfaces between any two adjacent layers deposited with successive transfers. The effect of these voids on the disconnections of the graphene layer after a number of bending cycles is evaluated in a later section.

Figure 3a–c shows the variations in electrical resistance with the number of bending cycles in the specimens prepared with 1, 2, and 3 transfers, respectively. The variations were obtained from the measurements of bending frequency at 0.5, 1.0, and 2.0 Hz, respectively. The initial electrical resistance R_o before bending depends on the number of graphene transfers; it decreases with increasing number of transfers, and thus the number and the total thickness of graphene layers. The electrical resistance only slightly increased for bending frequencies of 0.5 and 1.0 Hz. For a bending frequency of 2.0 Hz, the electrical resistance increased significantly after a few bending cycles, and its rate of increase strongly depended on the number of graphene transfers. The rate of increase varies with the number of bending cycles and is proportional to the number of graphene transfers. The results also suggest that with more number of graphene transfers, thus more number of PMMA residue or voids situated in between transferred layers, the electrical resistance will be effected more significantly.

Define R_o as the initial electrical resistance of the specimen before bending, and R as the electrical resistance varying with the bending cycles. Then, the rate of increase of electrical

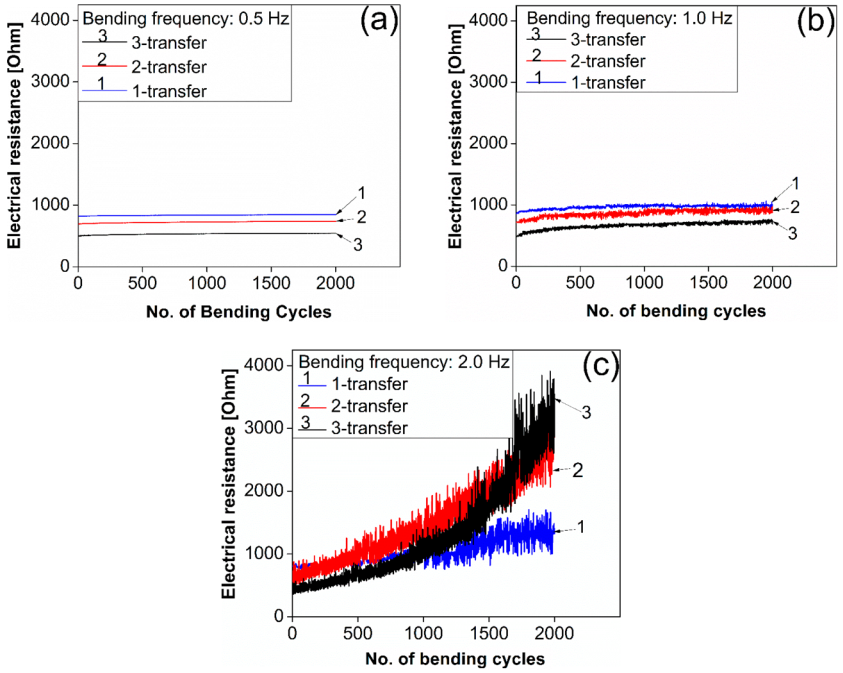

Figure 3. Electrical resistance variation for specimens with various graphene thicknesses versus number of bending cycles obtained at bending frequencies of (a) 0.5, (b) 1.0, and (c) 2.0 Hz.

dx.doi.org/10.1021/am5033154 | ACS Appl. Mater. Interfaces 2014, 6, 19566–19573

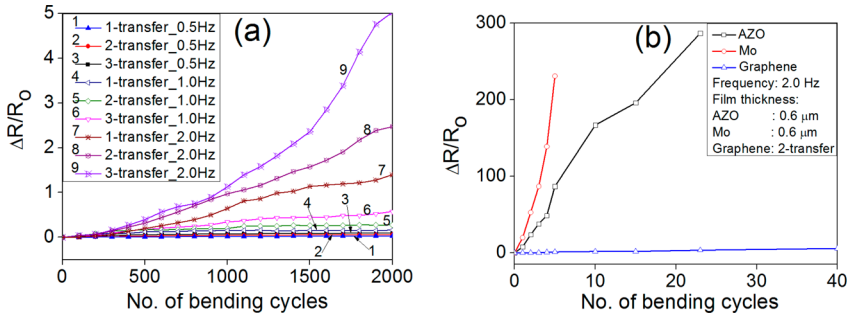

Figure 4. (a) Variation in mean rate of increase of electrical resistance $\Delta R/R_o$ with number of bending cycles. (b) Comparison of $\Delta R/R_o$ values for graphene/PI, Mo/PI, and AZO/PI specimens.

resistance ($\Delta R/R_o$) is defined as $(R - R_o)/R_o$. Figure 4a shows the variation in $\Delta R/R_o$ with the number of bending cycles for the three kinds of specimen at various bending frequencies. The $\Delta R/R_o$ values are strongly dependent on three factors: the number of graphene transfers, the bending frequency, and the number of bending cycles. If the number of graphene transfers and the bending frequency are fixed, the $\Delta R/R_o$ value increases with increasing number of bending cycles for all test conditions. If the number of bending cycles is fixed, a specimen prepared with a larger number of graphene transfers and tested at a higher bending frequency will have a higher value of $\Delta R/R_o$. Therefore, the $\Delta R/R_o$ value of the specimen prepared with three transfers bent at 2.0 Hz is much larger than those obtained in the other 8 test conditions. This is partly attributable to the fact that the specimen prepared with three transfers has the most voids. These voids are significantly enlarged after a number of bending cycles at the highest bending frequency. Figure 4b compares the variations of $\Delta R/R_o$ for three specimens with aluminum-doped zinc oxide (AZO), Mo, and graphene films, respectively, as the coating material. PI was used as the common substrate material. For a given bending frequency (2.0 Hz), the rate of increase of $\Delta R/R_o$ for the specimen with graphene is much lower than those of the other two specimens for a given number of bending cycles. The flexibility of graphene helps better resist void expansion during the cyclic bending process compared to the resistance offered by AZO and Mo.

Specimens prepared with different numbers of graphene transfers were tested at three bending frequencies. The cross-sectional morphologies of the specimens prepared with 1, 2, and 3 transfers after 2000 bending cycles at a bending frequency of 1.0 Hz are presented in Figure 5a–c, respectively. As shown in Figure 5a, a void enlarged to form a bulge, called an extrusion, such that some disconnections formed in the graphene layers. Interestingly, the three layers of graphene expanded simultaneously in the upward direction such that the size of the original void before the bending test increased significantly. Figure 5a shows that the larger void after the bending cycles actually resulted from the originally small void, which was produced during the transfer of graphene. Figure 5b shows the morphology of the specimen prepared with two transfers after 2000 bending cycles at the same bending frequency (1.0 Hz). There exists an enlarged void between the upper three layers and the lower three layers of graphene. The position of this void is exactly at the interface of the layers deposited with the first and second transfers, respectively. Therefore, it is believed that the expanded void after bending results from the evolution of the original void before bending. Figure 5c shows the cross-sectional morphology of the

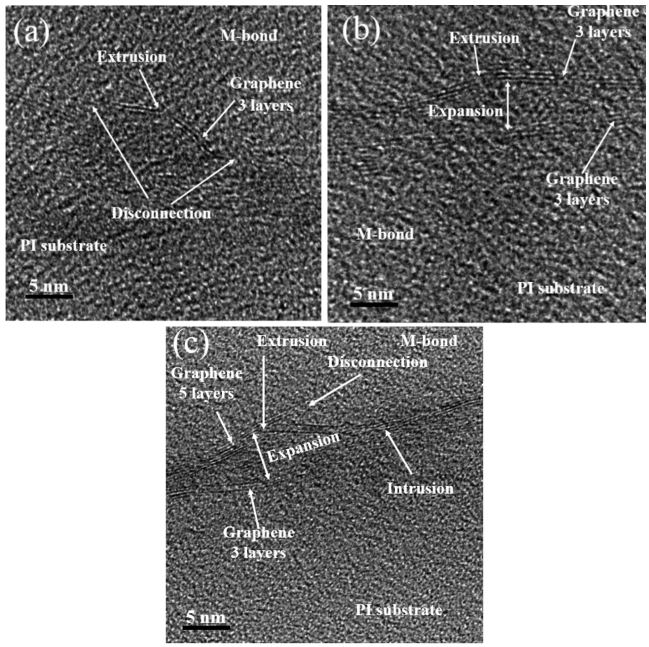

Figure 5. TEM morphologies of lateral surfaces of specimens prepared with (a) 1, (b) 2, and (c) 3 transfers after 2000 bending cycles at bending frequency of 1.0 Hz.

specimen prepared with three transfers (9 layers of graphene) after 2000 bending cycles at the same bending frequency. Voids are found at the interfaces formed by any two adjacent layers deposited with successive transfers. These voids make the graphene layers of every transfer disconnect at several places. These three figures prove that the expanded voids after bending resulted from the original small voids formed at the interfaces. This behavior was also found for the other two bending frequencies.

Raman spectroscopy measurements were carried out for all specimens before and after various bending cycles. In this study, 0, 500, 1000, 1500, and 2000 bending cycles were used. The peak positions and peak intensities of the D band, G band, and 2D band for all these measurements are listed in Table 1. The G and D peaks lie at around 1580 and 1350 cm^{-1}, respectively. The G peak corresponds to the double degenerate E_{2g} phonon at the Brillouin-zone center. The D peak is produced due to the breathing modes of sp^2 rings and requires a defect for its activation.[1,2] The D peak intensity is not related to the number of graphene layers but only to the amount of disorder.[1,2] The 2D peak is the second order the D peak; it lies at around 2691 cm^{-1}. The single 2D peak originates from a process where

dx.doi.org/10.1021/am5033154 | ACS Appl. Mater. Interfaces 2014, 6, 19566–19573

Table 1. Raman shifts and Reciprocal Lattice Constants for Specimen Prepared with Two Transfers after Bending Tests with Various Numbers of Bending cycles and Bending Frequencies

		D peak	G peak		2D peak		SAED reciprocal lattice	
frequency	no. of bending cycles	intensity (au)	position (cm^{-1})	intensity (au)	position (cm^{-1})	intensity (au)	L_1 (nm^{-1})	L_2 (nm^{-1})
0.5	0	negligibly small	1585	4157	2668	8646	4.74	4.74
	500	103	1585	4120	2668	8363	4.77	4.68
	1000	187	1583	3978	2667	8633	4.89	4.65
	1500	264	1582	3718	2665	8663	5.09	4.54
	2000	347	1580	3771	2662	7769	5.17	4.52
1.0	500	116	1584	4296	2666	9151	4.89	4.62
	1000	549	1581	3360	2663	7466	5.2	4.63
	1500	1321	1578	4003	2661	9407	5.47	4.68
	2000	2198	1574	4147	2656	9414	6.16	4.61
2.0	500	378	1582	4846	2664	11340	5.01	4.68
	1000	894	1577	4966	2659	9834	5.51	4.61
	1500	2475	1573	5755	2654	12202	5.83	4.65
	2000	4257	1567	4434	2646	10908	6.18	4.47

momentum conservation is obtained by the participation of one phonon with a wave vector of $\vec{q}$. It does not require the presence of defects for its activation and is thus always present. Figure 6 shows the Raman spectrum for the specimen prepared

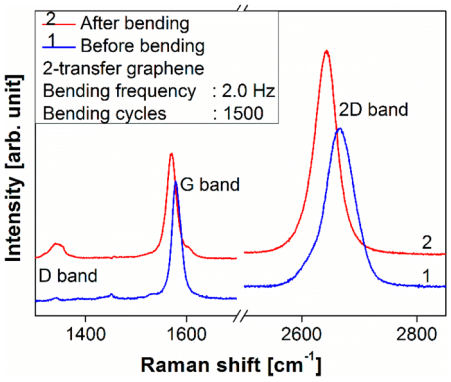

Figure 6. Raman Spectra of Specimen Prepared with Two Transfers before and after Bending Test.

with two transfers before and after bending. Before bending, two peaks are clearly visible between a Raman shift of 1000–3000 cm^{-1}, corresponding to the G band (~1585 cm^{-1}) and 2D band (~2668 cm^{-1}), respectively. The Raman shift shows that the peak corresponding to the D band (~1346 cm^{-1}) is negligibly small in the specimen before bending. The 2D structure of graphene is one of its most intriguing properties. A distinctive feature of the Raman spectrum is that the 2D band has a higher peak intensity than that of the G band.[12,13,26] The D-to-G intensity ratio of $I_D/I_G \approx 0.02$ indicates that the specimen prepared with two transfers before bending had a low defect density. The intensity of the D peak for this specimen after 2000 bending cycles is no longer negligibly small. In general, the D peak intensity strongly depends on the bending frequency and the number of bending cycles.

The peak positions and intensities of the D, G, and 2D bands for these three kinds of specimen obtained for five numbers of bending cycles and three bending frequencies are given in Table 1. These data show that the D peak Raman shift is invariant with the number of bending cycles, the bending frequency, and the graphene transfer number. However, the Raman shifts show that the peak positions of the G band and 2D band slightly decrease with increasing number of bending cycles for a given bending frequency. For a given number of bending cycles, the peak positions of these two bands both decrease with increasing bending frequency. The peak positions of these two bands are presented to be inversely, and are almost linearly proportional to the number of bending cycles and bending frequency. Therefore, the bending cycles lead to a blue shift. The compressive stress in the graphene film increased with increasing number of bending cycles and bending frequency.

The I_D/I_G ratios evaluated for specimen prepared with two transfers for three bending frequencies are shown in Figure 7a for various bending cycles. The peak intensity of I_G is almost independent of the bending frequency and the number of bending cycles. As mentioned previously, the I_D/I_G ratio is an indication of crystalline disorder or defect density.[8] At a fixed bending frequency, the I_D/I_G value increases with increasing

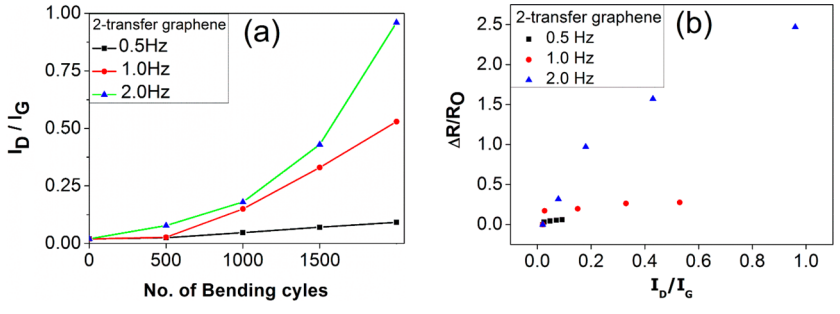

Figure 7. Variations of (a) I_D/I_G and (b) $\Delta R/R_o$ as a function of I_D/I_G for specimen prepared with two transfers.

dx.doi.org/10.1021/am5033154 | ACS Appl. Mater. Interfaces 2014, 6, 19566–19573

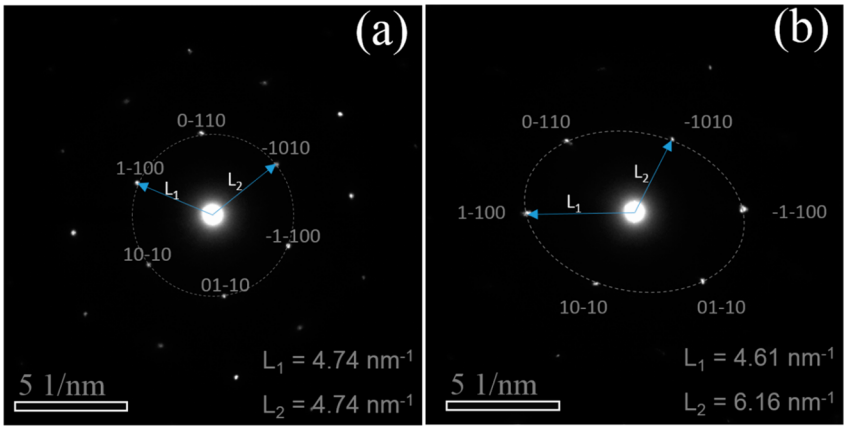

Figure 8. SAED pattern of graphene (a) before and (b) after bending tests.

number of bending cycles. A significant increase in I_D/I_G was observed at large bending frequencies and large numbers of bending cycles, which resulted in remarkable increases in void size and number of disconnection. The trend of the variation of I_D/I_G with the number of bending cycles demonstrated in Figure 7(a) is similar to that of the $\Delta R/R_o$ curves shown in Figure 4a labeled "2", "5", and "8". A nonlinear relationship was found for these three bending frequencies as shown in Figure 7b. The rate of increase in $\Delta R/R_o$ due to an increase in I_D/I_G is strongly dependent on the bending frequency; it increases nonlinearly with increasing bending frequency. This implies that bending with higher frequency generates more bending-induced disorder which significantly increased the value of $\Delta R/R_o$. The newly generated or enlarged voids, defects, extrusion, all boost the increasing rate of $\Delta R/R_o$. Frequency is related to the graphene's stress relaxation time. Generally, longer stress relaxation time depressed defect's creation. This phenomenon also applies to the specimens with 1 transfer and 3 transfers. It is thus concluded that the I_D value, or the defects density in graphene film is the governing factor of the rate of increase of the electrical resistance ($\Delta R/R_o$).

TEM SAED patterns were obtained for all specimens for various numbers of bending cycles. Figure 8a shows the SAED pattern for the specimen prepared with two transfers before bending. 6-fold hexagonal symmetry is clearly visible. The Bravais-Miller indices (*hkil*) were used to label the diffraction spots. The SAED patterns for the specimens after bending (Figure 8b) show an ellipse with L_2 as the half length of the short axis, and L_1 as the half length of the long axis. The variation of L_1 and L_2 values versus with the graphene transfer number, the number of bending cycles, and the bending frequency (data shown in Table 1).

The L_1/L_2 values for the specimen prepared with two transfers before and after various bending cycles were obtained to establish their relation to the I_D/I_G parameter. A monotonic relation was found between the I_D/I_G and L_1/L_2 parameters. Figure 9 shows the I_D/I_G and L_1/L_2 values obtained from the bending tests with the five numbers of bending cycles and three bending frequencies. For each bending frequency, the I_D/I_G value increase nonlinearly with the bending cycles. All the data associated with the three bending frequencies can be regressed roughly by a curve such that the I_D/I_G value can be determined as long as the value of L_1/L_2 is available. Because the lattice constants change significantly, the possible material change or lattice disorder was investigated using TEM SAED on an intentionally tilted sample without any bending history. Ellipse

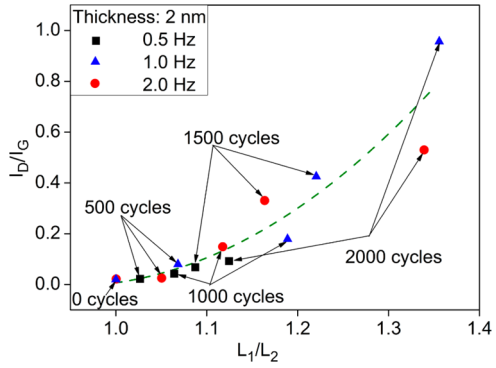

Figure 9. Variation of I_D/I_G with L_1/L_2 for specimen prepared with two transfers after 2000 bending cycles at three bending frequencies.

SAED patterns were also produced and the L_1/L_2 ratio varies with sample tilting angle. This suggests that the variations of L_1/L_2 obtained from the samples after bending tests are due to the diffraction patterns being obtained from nonflat graphene films.

The morphology of a specimen with graphene as the coating film shows thin parallel strips before bending. The turning angle is here defined as the angle between the orientations of the graphene strips formed on two sides of an extrusion. Therefore, the turning angle before bending is 180°. After a number of bending cycles, extrusions and intrusions appear, and the new graphene strips are orientated at a small angle with respect to the original graphene strips. The magnitude of the turning angle is dependent on the number of bending cycles, bending frequency, and number of graphene transfers. In the present study, the measurements of turning angle were made for an extrusion formed at the same position in all specimens. Figure 10a1−a4 shows the morphologies of the specimen prepared with two transfers obtained from tests with 500, 1000, 1500, and 2000 bending cycles, respectively, at a bending frequency of 2.0 Hz. Figure 10b shows the turning angles varying with the number of bending cycles and bending frequency for the specimen prepared with two transfers for three bending frequencies. The data show that the turning angle decreased with increasing number of bending cycles for a given bending frequency. A lower turning angle indicates more damage on the graphene strips and more defects generated by the bending. For a given number of bending cycles, an increase in the bending frequency decreased the turning angle. This also applies to the other two specimens with different graphene

dx.doi.org/10.1021/am5033154 | ACS Appl. Mater. Interfaces 2014, 6, 19566−19573

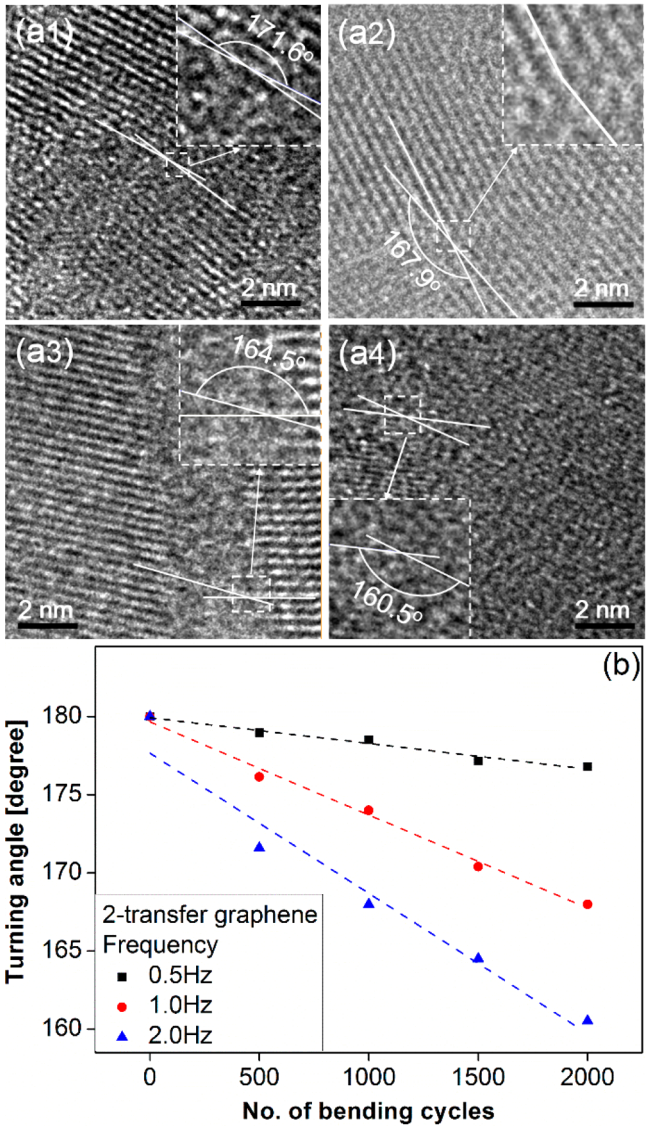

Figure 10. (a) TEM morphologies for measurement of tilt angle of specimen prepared with two transfers after bending tests with (1) 500, (2) 1000, (3) 1500, and (4) 2000 cycles obtained at bending frequency of 2.0 Hz. (b) Variations in turning angle with number of bending cycles and bending frequency.

thicknesses. An increase in the graphene transfer number (or thickness) can bring in a reduction in the turning angle, especially at high bending frequency.

The TEM morphology of the lateral surface of the specimen was acquired to evaluate the tilt angle of the top graphene layer as a function of bending test frequency. The tilt angle is defined as the angle between the incline surface of the top graphene layer and the undeformed surface of the same graphene layer. Figure 11 shows the tilt angles for the specimen with different graphene transfer at three bending frequencies obtained after 2000 bending cycles. The tilt angle increases with the number of the graphene transfer. The tilting angle could be caused by the formation of extrusions/intrusions, it also depends on how well the grapheme was transferred, the number of bending cycles, and the bending frequency.

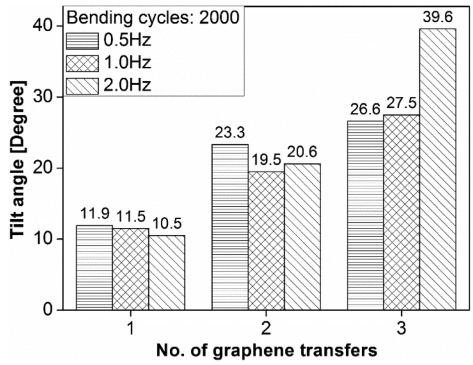

Figure 11. Tilt angles obtained from lateral surfaces of specimens after 2000 bending cycles at three bending frequencies.

CONCLUSIONS

In summary, shuttle-shaped voids formed at the interfaces between any two adjacent graphene layers deposited by successive graphene transfers. Graphene transfer onto the substrate are responsible for the subsequent size enlargement of voids and the resulting disconnections or extrusions of the graphene layers whose increasing bending cycles. Electrical resistance (R) and thus its rate of increase ($\Delta R/R_o$) are strongly dependent on the quantities of these voids and disconnections. In general, $\Delta R/R_o$ increases as the number of graphene transfers, the number of bending cycles, and the bending frequency increase.

The I_D peak intensity of the Raman spectra for the specimens before bending is negligibly small. It increases significantly after the bending tests. For a specimen with a given graphene thickness, the I_D/I_G value increases exponentially with increasing number of bending cycles and bending frequency. The rate of increase of electrical resistance, $\Delta R/R_o$, increases with increasing I_D/I_G, becomes significantly when bending is applied with sufficiently high frequency. In addition, the I_D/I_G ratio nonlinearly increases with the L_1/L_2 ratio measured from the SAED patterns. Changes of L_1/L_2 ratio is related to nonflat graphene surface after bending.The value of the tilt angle formed in the top graphene layer of the specimen after 2000 bending cycles depends on the number of graphene transfer and the bending frequency. For a given bending frequency, the tilt angle increases with increasing number of graphene transfer. The turning angle due to severe extrusion/intrusion decreases with increasing the number of graphene transfers, number of bending cycles, or bending frequency.

AUTHOR INFORMATION

Corresponding Author

*E-mail: jflin@mail.ncku.edu.tw.

Notes

The authors declare no competing financial interest.

REFERENCES

(1) Coraux, J.; N'Diaye, A. T.; Busse, C.; Michely, T. Structural Coherency of Ggraphene on Ir(111). *Nano Lett.* **2008**, *8*, 565−570.

(2) Kim, K. S.; Zhao, Y.; Jang, H.; Lee, S. Y.; Kim, J. M.; Kim, S. S.; Ahn, J. H.; Kim, P.; Choi, J. Y.; Hong, B. H. Large-Scale Pattern Growth of Graphene Films for Stretchable Transparent Electrodes. *Nature* **2009**, *457*, 706−710.

(3) Lee, Y. B.; Bae, S. K.; Jang, H.; Jang, S. K.; Zhu, S. E.; Sim, S. H.; Song, Y. I.; Hong, B. H.; Ahn, J. H. Wafer-Scale Synthesis and Transfer of Graphene Films. *Nano Lett.* **2010**, *10*, 490−493.

(4) Reina, A.; Son, H. B.; Jiao, L. Y.; Fan, B.; Dresselhaus, M. S.; Liu, Z. F.; Kong, J. Transferring and Identification of Single- and Few-Layer Graphene on Arbitrary Substrates. *J. Phys. Chem. C* **2008**, *112*, 17741−17744.
(5) Li, X. S.; Zhu, Y. W.; Cai, W. W.; Borysiak, M.; Han, B. Y.; Chen, D.; Piner, R. D.; Colombo, L.; Ruoff, R. S. Transfer of Large-Area Graphene Films for High-Performance Transparent Conductive Electrodes. *Nano Lett.* **2009**, *9*, 4359−4363.
(6) Hao, Y.; Bharathi, M. S.; Wang, L.; Liu, Y.; Chen, H.; Nie, S.; Wang, X.; Chou, H.; Tan, C.; Fallahazad, B.; Ramanarayan, H.; Magnuson, C. W.; Tutuc, E.; Yakobson, B. I.; McCarty, K. F.; Zhang, Y. W.; Kim, P.; Hone, J.; Colombo, L.; Ruoff, R. S. The Role of Surface Oxygen in the Growth of Large Single-Crystal Graphene on Copper. *Science* **2013**, *342*, 720−723.
(7) Li, X. S.; Cai, W. W.; An, J. H.; Kim, S.; Nah, J.; Yang, D. X.; Piner, R. D.; Velamakanni, A.; Jung, I.; Tutuc, E.; Banerjee, S. K.; Colombo, L.; Ruoff, R. S. Large-Area Synthesis of High-Quality and Uniform Graphene Films on Copper Foils. *Science* **2009**, *324*, 1312−1314.
(8) Lee, S. H.; Lee, K. H.; Zhong, Z. H. Wafer Scale Homogeneous Bilayer Graphene Films by Chemical Vapor Deposition. *Nano Lett.* **2010**, *10*, 4702−4707.
(9) Bae, S.; Kim, H.; Lee, Y.; Xu, X.; Park, J. S.; Zheng, Y.; Balafrishnan, J.; Lei, T.; Kim, H. R.; Song, Y. I.; Kim, Y. J.; Kim, K. S.; Özyilmaz, B.; Ahn, J. H.; Hong, B. H.; Lijima, S. Roll-to-Roll Production of 30-in. Graphene Films for Transparent Electrodes. *Nat. Nanotechnol.* **2010**, *5*, 574−578.
(10) Tsen, A. W.; Brown, L.; Levendorf, M. P.; Ghahari, F.; Huang, P. Y.; Havener, R. W.; Ruiz-Vargas, C. S.; Muller, D. A.; Kim, P.; Park, J. Tailoring Electrical Transport across Grain Boundaries in Polycrystalline Graphene. *Science* **2012**, *336*, 1143−1146.
(11) Kim, K.; Lee, H. B. R.; Johnson, R. W.; Tanskanen, J. T.; Liu, N.; Kim, M. G.; Pang, C.; Ahn, C.; Bent, S. F.; Bao, Z. Selective Metal Deposition at Graphene Line Defects by Atomic Layer Deposition. *Nat. Commun.* **2014**, *5*, 4781.
(12) Malard, L. M.; Pimenta, M. A.; Dresselhaus, G.; Dresselhaus, M. S. Raman Spectroscopy in Graphene. *Phys. Rep.* **2009**, *473*, 51−87.
(13) Graf, D.; Molitor, F.; Ensslin, K.; Stampfer, C.; Jungen, A.; Hierold, C.; Wirtz, L. Spatially Resolved Raman Spectroscopy of Single- and Few-Layer Graphene. *Nano Lett.* **2007**, *7*, 238−242.
(14) Ferrari, A. C.; Meyer, J. C.; Scardaci, V.; Casiraghi, C.; Lazzeri, M.; Mauri, F.; Piscanec, S.; Jiang, D.; Novoselov, K. S.; Roth, S.; Geim, A. K. Raman Spectrum of Graphene and Graphene Layers. *Phys. Rev. Lett.* **2006**, *97*, 187401.
(15) Hao, Y.; Wang, Y.; Wang, L.; Ni, Z.; Wang, Z.; Wang, R.; Koo, C. K.; Shen, Z.; Thong, J. T. Probing Layer Number and Stacking Order of Few-Layer Graphene by Raman spectroscopy. *Small* **2010**, *6*, 195−200.
(16) Scarpa, F.; Adhikari, S.; Srikantha Phani, A. Effective Elastic Mechanical Properties of Single Layer Graphene Sheets. *Nanotechnology* **2009**, *20*, 065709.
(17) Ni, Z. H.; Yu, T.; Lu, Y. H.; Wang, Y. Y.; Feng, Y. P.; Shen, Z. X. Uniaxial Strain on Graphene: Raman Spectroscopy Study and Band-Gap Opening. *ACS Nano* **2008**, *2*, 2301−2305.
(18) Mohiuddin, T. M. G.; Lombardo, A.; Nair, R. R.; Bonetti, A.; Savini, G.; Jalil, R.; Bonini, N.; Basko, D. M.; Galiotis, C.; Marzari, N.; Novoselov, K. S.; Geim, A. K.; Ferrari, A. C. Uniaxial Strain in Graphene by Raman Spectroscopy: G Peak Splitting, Grüneisen Parameters, and Sample Orientation. *Phys. Rev. B: Condens. Matter Mater. Phys.* **2009**, *79*, 205433.
(19) Yu, T.; Ni, Z. H.; Du, C. L.; You, Y. M.; Wang, Y. Y.; Shen, Z. X. Raman Mapping Investigation of Graphene on Transparent Flexible Substrate: The Strain Effect. *J. Phys. Chem. C* **2008**, *112*, 12602−12605.
(20) Cranford, S. W.; Buehler, M. J. Mechanical Properties of Graphyne. *Carbon* **2011**, *49*, 4111−4121.
(21) Warner, J. H.; Margine, E. R.; Mukai, M.; Robertson, A. W.; Giustino, F.; Kirkland, A. I. Dislocation-Driven Deformations in Graphene. *Science* **2012**, *337*, 209−212.
(22) Frank, O.; Vejpravova, J.; Kavan, L.; Kalbac, M. Raman Spectroscopy Investigation of Defect Occurrence in Graphene Grown on Copper Single Crystals. *Phys. Status Solidi B* **2013**, *250*, 2497−2766.
(23) Polák, J.; Sauzay, M. Growth of Extrusions in Localized Cyclic Plastic Straining. *Mater. Sci. Eng., A* **2009**, *500*, 122−129.
(24) Avouris, P.; Chen, Z.; Perebeinos, V. Carbon-Based Electronics. *Nat. Nanotechnol.* **2007**, *2*, 605−615.
(25) Li, T. C.; Han, C. F.; Chen, K. T.; Lin, J. F. Fatigue Life Study of ITO/PET Specimens in Terms of Electrical Resistance and Stress/Strain Via Cyclic Bending Tests. *J. Disp. Technol.* **2013**, *9*, 577−585.
(26) Berciaud, S.; Ryu, S.; Brus, L. E.; Heinz, T. F. Probing the Intrinsic Properties of Exfoliated Graphene: Raman Spectroscopy of Free-Standing Monolayers. *Nano Lett.* **2009**, *9*, 346−352.